Neuron, Volume *72*

Supplemental Information

Functional Specialization of Seven Mouse Visual Cortical Areas

James H. Marshel, Marina E. Garrett, Ian Nauhaus, and Edward M. Callaway

Supplemental Information

I. Supplemental Data

Area	Total Neurons		Responsive Neurons		Reliable Neurons		Responsive & Reliable		Included Neurons		*N* Expts	
	SF	TF	SF	TF	SF	TF	SF	TF	SF	TF	SF	TF
	N	*N*	*N (% Total)*	*N (% Total)*	*N (% Total)*	*N (% Total)*	*N (% Total)*	*N (% Total)*	*N (% Total)*	*N (% Total)*	*N*	*N*
V1	1419	1382	826 (58%)	718 (52%)	1063 (75%)	984 (71%)	728 (51%)	586 (42%)	728 (51%)	584 (42%)	11	10
LM	590	584	328 (56%)	198 (34%)	495 (84%)	404 (69%)	300 (51%)	171 (29%)	295 (50%)	171 (29%)	7	7
LI	182	193	51 (28%)	35 (18%)	85 (47%)	56 (29%)	42 (23%)	23 (12%)	40 (22%)	23 (12%)	2	2
AL	890	918	418 (47%)	343 (37%)	541 (61%)	542 (59%)	330 (37%)	257 (28%)	323 (36%)	253 (28%)	6	6
RL	616	555	232 (38%)	124 (22%)	382 (62%)	295 (53%)	201 (33%)	96 (17%)	194 (31%)	95 (17%)	6	6
AM	404	311	80 (20%)	25 (8%)	203 (50%)	70 (23%)	63 (16%)	12 (4%)	63 (16%)	11 (4%)	6	6
PM	508	506	172 (34%)	78 (15%)	332 (65%)	230 (45%)	147 (29%)	50 (10%)	147 (29%)	50 (10%)	3	3
Total	4609	4449	2107 (46%)	1521 (34%)	3101 (67%)	2581 (58%)	1811 (39%)	1195 (27%)	1790 (39%)	1187 (27%)	41	40

Table S1, related to Table 1. Further tabulation of numbers of neurons sampled by cortical area. Total neurons indicates number (*N*) of neurons recorded in the spatial frequency (SF) and temporal frequency (TF) experiments for each area. Number (*N*) and percent of total of responsive ($\Delta F/F > 6\%$) and reliable neurons ($\delta > 1$, Experimental Procedures) for each area. Neurons which were responsive and reliable, as well as representing eccentricities within 50° of the center of space (over 99% of responsive and reliable neurons) were included in subsequent population analyses. "*N* Expts" refers to the number of fields of view (samples of neurons) recorded from for each area. This table (compared to Table 1) separates responsive from reliable criteria, and shows number of neurons passing eccentricity criteria for inclusion in our analysis.

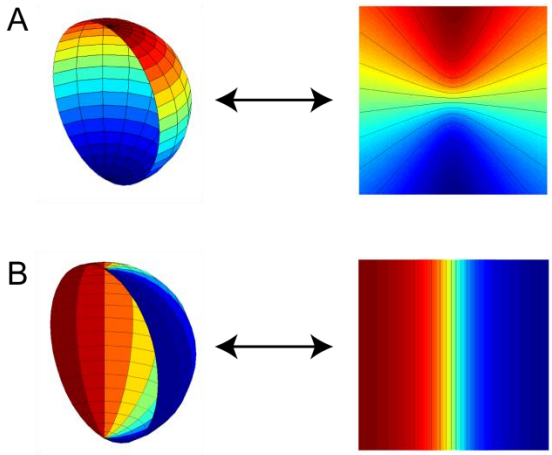

Figure S1, Related to Figure 1. Spherical coordinates transformed to a flat surface. A mathematical transformation (Supplemental Experimental Procedures) was applied to all stimuli so that they were displayed in spherical coordinates on a flat monitor (tangent to the hemisphere). **(A)** Altitude coordinates. Colors represent isoaltitude lines. This transformation was applied to drifting sine wave grating stimuli in order to keep spatial and temporal frequencies constant throughout the hemifield. It was also applied to vertical retinotopy stimuli (Movie S1). **(B)** Azimuth coordinates. Colors represent isoazimuth lines. This transformation was applied to horizontal retinotopy stimuli (Movie S2). The combination of altitude and azimuth-corrected retinotopy stimuli mapped retinotopic eccentricity in spherical coordinates using a flat monitor.

Figure S2

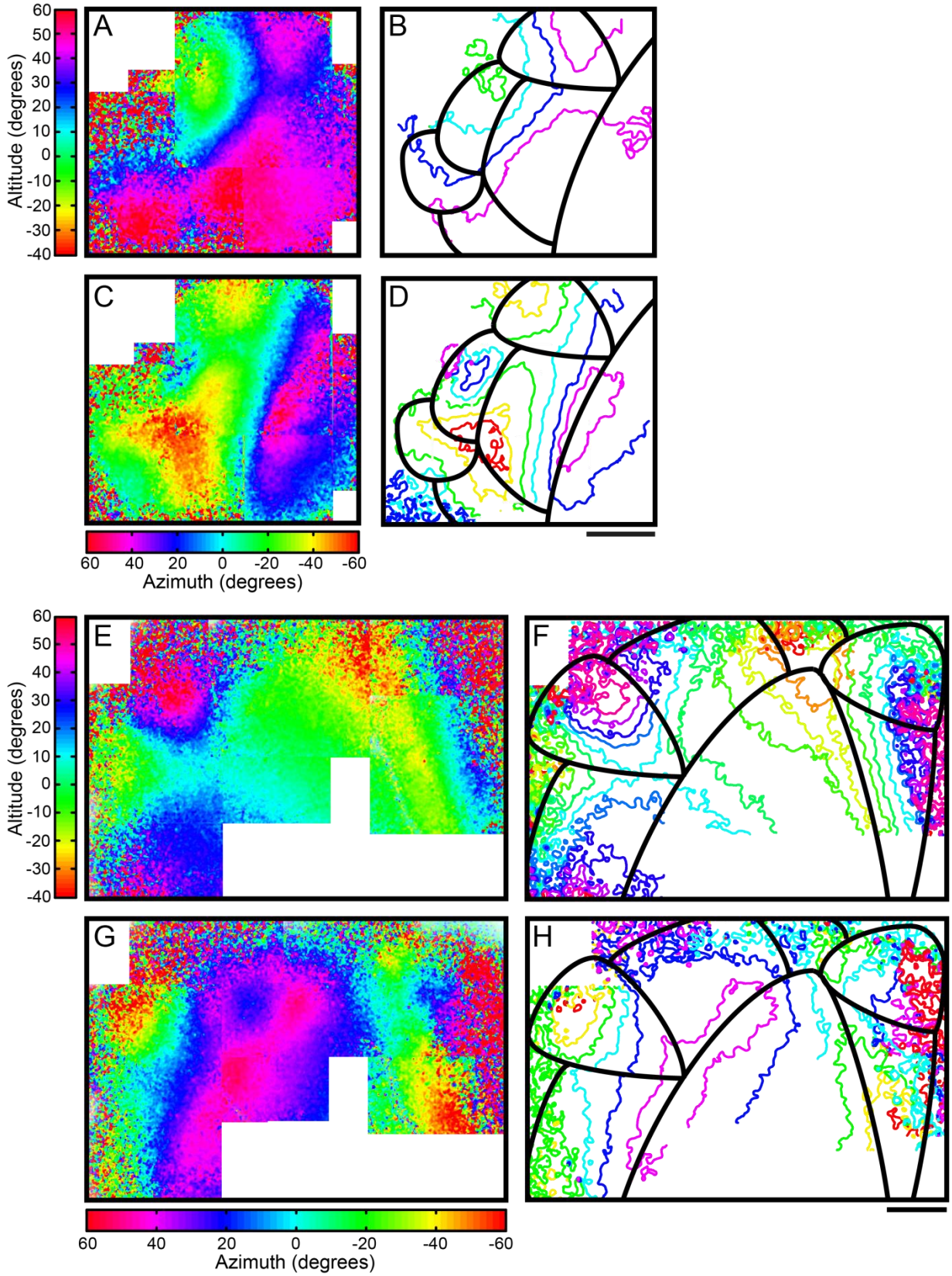
A
B
C
D
E
F
G
H
Altitude (degrees)
60
50
40
30
20
10
0
-10
-20
-30
-40
Azimuth (degrees)
60
40
20
0
-20
-40
-60

Figure S2, related to Figure 2. High-resolution retinotopic maps measured with low magnification two-photon calcium imaging reveal structural details of small visual areas. Fine-scale retinotopic organization of mouse visual cortex (A-H). Colors represent retinotopic eccentricity, as in Figure 2. Panels A & E show continuous vertical retinotopy maps, in altitude coordinates. Positive values indicate the upper field and negative values the lower field. Panels B & F show the corresponding contour plots of vertical eccentricity with area borders outlined in black. Panels C & G show continuous horizontal retinotopy maps, in azimuth coordinates, with positive values representing the nasal visual field and negative values representing the temporal visual field. Panels D & H show contour plots of horizontal retinotopy, overlaid with area borders. Area borders correspond to area diagram in Figure 1I. **(A-D)** Retinotopic organization of posterior-lateral extrastriate areas. The retinotopic structures of areas P and POR, often difficult to resolve using intrinsic imaging, are revealed by mapping with calcium imaging. Areas shown in (B, D) correspond to V1, AL, LI, POR, and P surrounding area LM counterclockwise.. The border between V1 and LM and AL is marked by a reversal at the vertical meridian (blue-purple, (C, D)). LM and LI are separated by a reversal at the temporal periphery (yellow-green, (C,D)). AL is separated from LM by a reversal near the horizontal meridian (purple-blue (A, B)). A reversal in horizontal retinotopy separates both P and POR from areas LM and LI (yellow-red, (C,D)). The border between P and POR occurs at the representation of the upper periphery (purple (A, B)). **(E-H)** Retinotopic organization of anterior extrastriate areas, located in the posterior parietal cortex. Areas shown in (F, H) include LM, AL, RL, A, AM, PM, V1 (starting at lower left, moving clockwise). The retinotopic structure of all areas is consistent with maps displayed in Figure 2. Fine-scale features resolved by calcium imaging include a ring like structure in the representation of the vertical meridian in area RL (purple, (G, H)), as well as an organized representation of the visual field in both the horizontal and vertical dimension for areas AM and PM (right, (F, H)). Here, visual activation is observed in the expected location of area A, however, a clear retinotopic structure is not apparent. This area receives less-organized (less topographic) input from V1 than the other areas (Wang and Burkhalter 2007). All scale bars 500 µm.

Figure S3

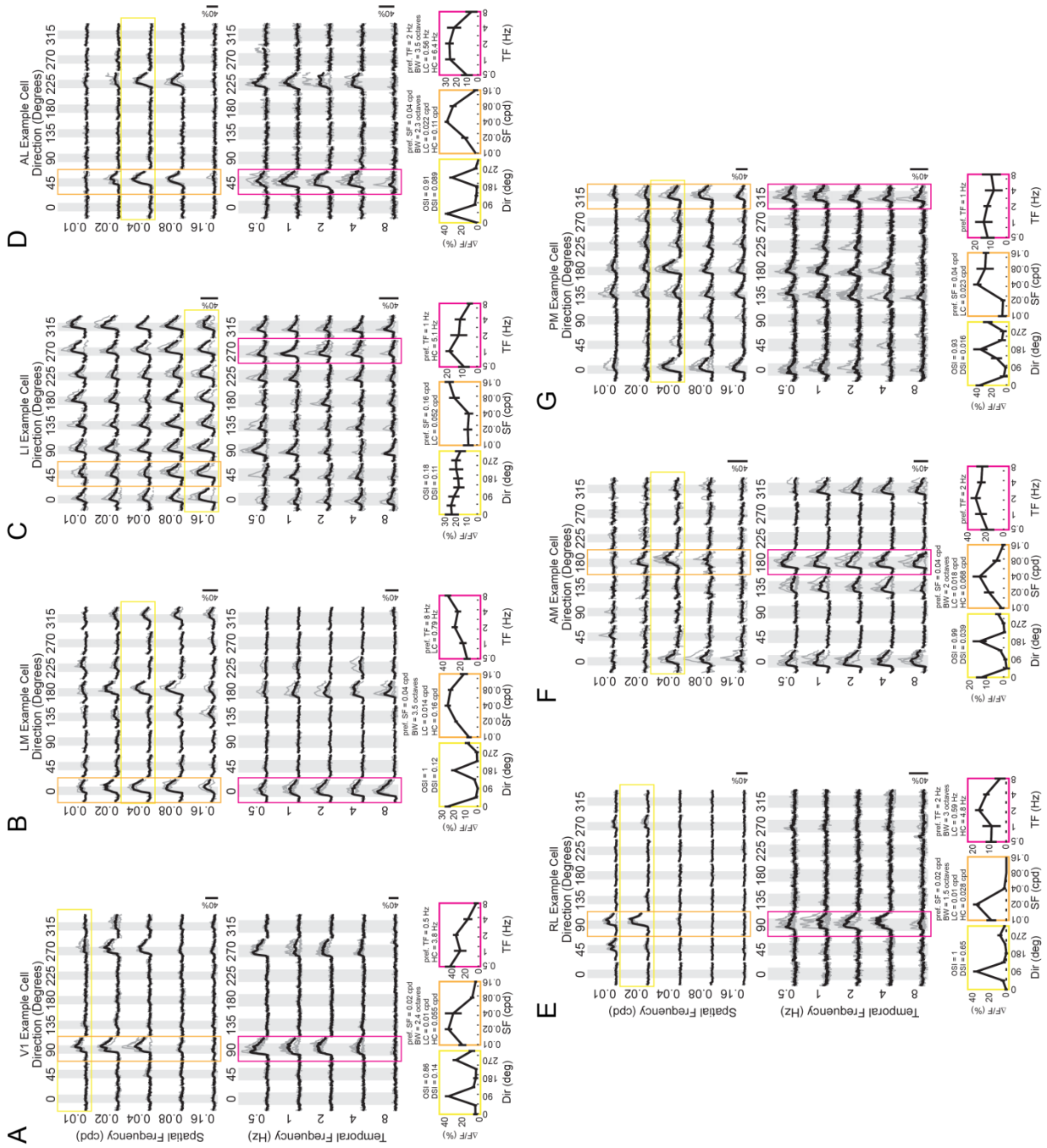
A
V1 Example Cell
Direction (Degrees)
Spatial Frequency (cpd)
Temporal Frequency (Hz)
OSI = 0.86
DSI = 0.14
pref. SF = 0.02 cpd
BW = 2.4 octaves
LC = 0.01 cpd
HC = 0.055 cpd
pref. TF = 0.5 Hz
HC = 3.8 Hz
B
LM Example Cell
OSI = 1
DSI = 0.12
pref. SF = 0.04 cpd
BW = 3.5 octaves
LC = 0.014 cpd
HC = 0.16 cpd
pref. TF = 8 Hz
LC = 0.79 Hz
C
LI Example Cell
OSI = 0.18
DSI = 0.11
pref. SF = 0.16 cpd
LC = 0.052 cpd
pref. TF = 1 Hz
HC = 5.1 Hz
D
AL Example Cell
OSI = 0.91
DSI = 0.089
pref. SF = 0.04 cpd
BW = 2.3 octaves
LC = 0.022 cpd
HC = 0.11 cpd
pref. TF = 2 Hz
BW = 3.5 octaves
LC = 0.56 Hz
HC = 6.4 Hz
E
RL Example Cell
OSI = 1
DSI = 0.65
pref. SF = 0.02 cpd
BW = 1.5 octaves
LC = 0.01 cpd
HC = 0.028 cpd
pref. TF = 2 Hz
BW = 3 octaves
LC = 0.39 Hz
HC = 4.8 Hz
F
AM Example Cell
OSI = 0.99
DSI = 0.039
pref. SF = 0.04 cpd
BW = 2 octaves
LC = 0.018 cpd
HC = 0.088 cpd
pref. TF = 2 Hz
G
PM Example Cell
OSI = 0.93
DSI = 0.016
pref. SF = 0.04 cpd
LC = 0.023 cpd
pref. TF = 1 Hz
ΔF/F (%)
Dir (deg)
SF (cpd)
TF (Hz)
40%

Figure S3, related to Figure 3. Responses are robust and selective across visual areas. Calcium responses and tuning curves for example cells from each visual area. Response matrices (upper plots) show the change in fluorescence over baseline for each stimulus condition, for the spatial frequency (SF) experiment (top of each panel) and temporal frequency (TF) experiment (middle of each panel). The average response across all trials of a given condition is shown in black, with the responses to each trial in gray. Gray boxes indicate the duration of the stimulus, 2 seconds for SF experiments, 4 seconds for TF experiments. Scale bars to lower right of matrices correspond to 40% $\Delta F/F$. Tuning curves (bottom of each panel) were generated by taking the average $\Delta F/F$ for each stimulus condition, at the intersection of the matrix that gave the peak response. Orientation tuning curves (yellow boxes) are taken across all orientations at the preferred spatial frequency, spatial frequency tuning curves (orange boxes) are taken across all spatial frequencies at the preferred orientation, and temporal frequency tuning curves (magenta boxes) are taken across all temporal frequencies at the preferred orientation. Values for preferred stimuli and selectivity metrics are listed above each tuning curve. OSI = orientation selectivity index, DSI = direction selectivity index, LC = low cutoff frequency, HC = high cutoff frequency, BW = bandwidth. **(A)** Example cell from V1. This cell is highly orientation selective, is bandpass for spatial frequency and lowpass for temporal frequency, preferring the lowest TF tested (0.5 Hz). **(B)** Example cell from LM. This cell is perfectly orientation selective (OSI = 1), bandpass for spatial frequency with broad tuning (BW = 3.5 octaves), and highpass for temporal frequency, preferring the highest temporal frequency tested (8 Hz). **(C)** Example cell from LI. This cell is broadly tuned for orientation, responding similarly to all orientations across all stimulus conditions (OSI = 0.18) and prefers high spatial frequencies (highpass, pref. SF = 0.16 cpd), and low temporal frequencies (1 Hz). **(D)** Example cell from AL. This cell is highly orientation selective, bandpass for spatial frequency with moderately sharp tuning (BW = 2.3 octaves) and broadly tuned for temporal frequency (BW= 3.5 octaves). **(E)** Example cell from RL. This cell is highly selective for direction, responding primarily to only one direction of motion for the same orientation (DSI = 0.65), and is highly selective for spatial frequency, with a bandwidth of 1.5 octaves. **(F)** Example cell from AM. This cell is orientation selective, has moderate spatial frequency selectivity (pref. SF = 0.4cpd, BW = 2 octaves), and responds similarly to all temporal frequencies. **(G)** Example cell from PM. This cell is orientation selective, is highpass for spatial frequency, and responds weakly across temporal frequencies.

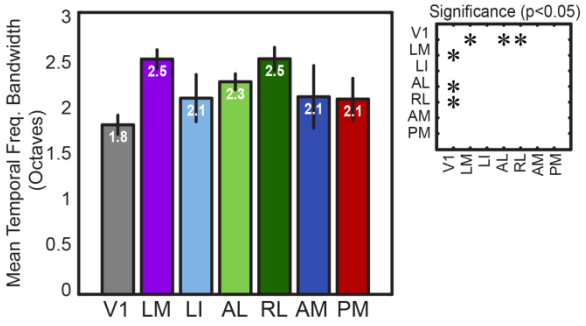

Figure S4, related to Figure 4. Mean temporal frequency bandwidth across visual areas. Mean temporal frequency bandwidth (in octaves) is higher in several extrastriate areas (LM, AL, RL) compared to V1, indicating that neurons in these areas respond to a broader range of temporal frequencies on average. Inset, statistical significance ($p < 0.05$) of pair-wise comparisons between areas, corrected for multiple comparisons by the Tukey-Kramer method. Error bars are standard error of the mean (S.E.M.).

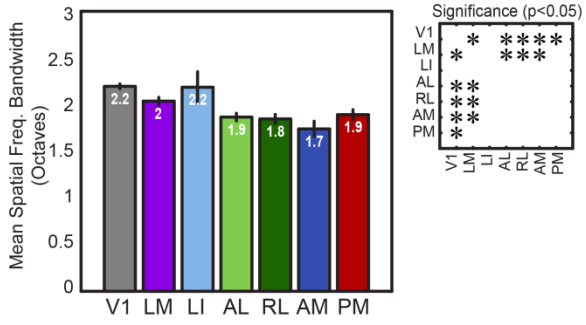

Figure S5, related to Figure 5. Mean spatial frequency bandwidth across visual areas. Mean spatial frequency bandwidth (in octaves) is sharper in all extrastriate areas except LI, indicating that higher visual areas are more selective for spatial frequency than V1. Further, some extrastriate areas (AL, RL, AM) have significantly sharper bandwidth values than LM. Inset, statistical significance ($p < 0.05$) of pair-wise comparisons between areas, corrected for multiple comparisons by the Tukey-Kramer method. Error bars are standard error of the mean (S.E.M.).

Figure S6

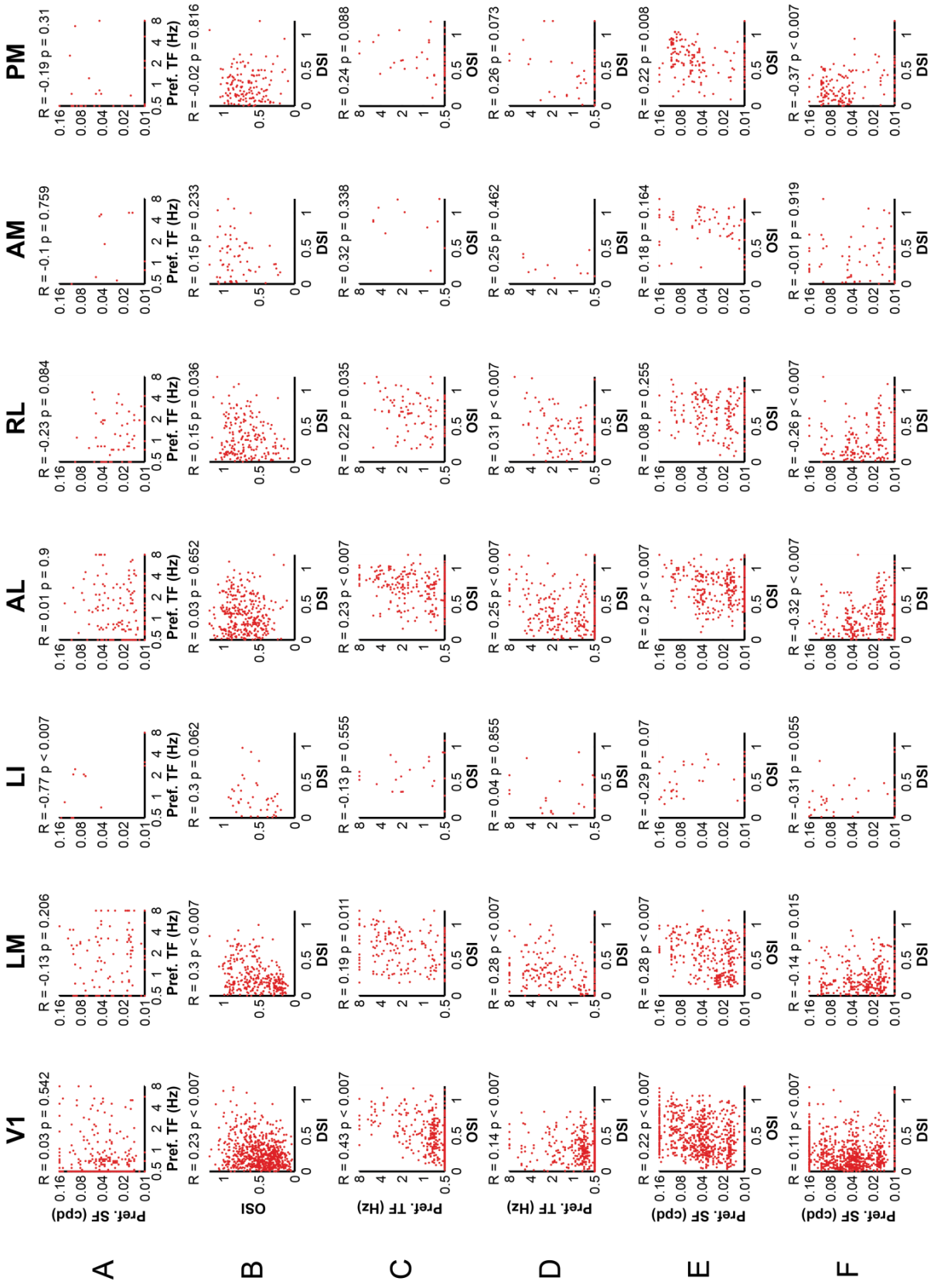
V1
LM
LI
AL
RL
AM
PM
A
B
C
D
E
F
Pref. SF (cpd)
OSI
Pref. TF (Hz)
Pref. TF (Hz)
Pref. SF (cpd)
Pref. SF (cpd)
R = 0.03 p = 0.542
R = -0.13 p = 0.206
R = -0.77 p < 0.007
R = 0.01 p = 0.9
R = -0.23 p = 0.084
R = -0.1 p = 0.759
R = -0.19 p = 0.31
Pref. TF (Hz)
R = 0.23 p < 0.007
R = 0.3 p < 0.007
R = 0.3 p = 0.062
R = 0.03 p = 0.652
R = 0.15 p = 0.036
R = 0.15 p = 0.233
R = -0.02 p = 0.816
DSI
R = 0.43 p < 0.007
R = 0.19 p = 0.011
R = -0.13 p = 0.555
R = 0.23 p < 0.007
R = 0.22 p = 0.035
R = 0.32 p = 0.338
R = 0.24 p = 0.088
OSI
R = 0.14 p < 0.007
R = 0.28 p < 0.007
R = 0.04 p = 0.855
R = 0.25 p < 0.007
R = 0.31 p < 0.007
R = 0.25 p = 0.462
R = 0.26 p = 0.073
R = 0.22 p < 0.007
R = 0.28 p < 0.007
R = -0.29 p = 0.07
R = 0.2 p < 0.007
R = 0.08 p = 0.255
R = 0.18 p = 0.164
R = 0.22 p = 0.008
R = 0.11 p < 0.007
R = -0.14 p = 0.015
R = -0.31 p = 0.055
R = -0.32 p < 0.007
R = -0.26 p < 0.007
R = -0.01 p = 0.919
R = -0.37 p < 0.007

Figure S6, related to Figure 7. Correlation analyses between each pair of metrics on a cell-by-cell basis for each area. Scatter plots of neuron scores for each combination of selectivity metrics for each area. Area names at top of figure correspond to the entire column of scatter plots. Pearson's correlation coefficients (R) are listed above each plot for each area, along with the p value corresponding to a significance test against zero correlation ($\alpha < 5\%$ for $p < 0.007$ after accounting for multiple comparisons with the Bonferroni method). **(A)** The preferred spatial frequency of each neuron is plotted as a function of preferred temporal frequency of each neuron for each area. Note: not all neurons in our dataset received scores for both spatial and temporal frequencies (e.g., we did not record from them in both experiments), thus the populations in the plots in (A) are a subset of the populations used in other analyses of SF and TF experiments alone. **(B)** The orientation selectivity index (OSI) of each neuron is plotted as a function of direction selectivity index (DSI) of each neuron for each area. **(C)** Preferred temporal frequency of each neuron is plotted as a function of OSI of each neuron for each area. **(D)** Preferred temporal frequency of each neuron plotted as a function of DSI of each neuron for each area. **(E)** Preferred spatial frequency of each neuron plotted as a function of OSI of each neuron for each area. **(F)** Preferred spatial frequency of each neuron as a function of DSI of each neuron for each area.

Movie S1, related to Figure 1. Vertical retinotopy visual stimulus. To map vertical retinotopy, a single bar was drifted across the full upper-lower extent of the visual hemifield while intrinsic signals or calcium transients were measured from the brain. An altitude spherical correction was applied to accurately project spherical coordinates onto a flat monitor. This gives the impression of a bar that is curved on the flat screen, but when observed at the appropriate distance, and with infinite focus (as in the mouse preparation) the bar defines altitude lines on a sphere. See Supplemental Experimental Procedures for details on stimulus parameters.

Movie S2, related to Figure 1. Horizontal retinotopy visual stimulus. To map horizontal retinotopy, a single bar was drifted across the full nasal-temporal extent of the visual hemifield while intrinsic signals or calcium transients were measured from the brain. An azimuth spherical correction was applied to accurately project spherical coordinates onto a flat monitor. This gives the impression of a bar that modulates in width on the flat screen, but when observed at the

appropriate distance, and with infinite focus (as in the mouse preparation) the bar defines azimuth lines on a sphere. See Supplemental Experimental Procedures for details on stimulus parameters.

II. Supplemental Experimental Procedures

Animal Preparation and Surgery

All experiments involving living animals were approved by the Salk Institute's Institutional Animal Care and Use Committee. All experiments were performed using C57BL/6 mice (n = 28) between 2 and 3 months of age. Surgical plane anesthesia was induced and maintained with isoflurane (2-2.5% induction, 1-1.25% surgery). Dexamethasone and carprofen were administered subcutaneously (2 mg/kg and 5 mg/kg respectively). Ibuprofen (30 mg/kg) was administered post-operatively in the drinking water if the animal recovered overnight after implanting the recording chamber. A custom-made metal chamber was mounted to the skull, centered on the visual cortex of the left hemisphere using stereotaxic coordinates. The frame was mounted so that it was as close to the skull as possible, tilted to be tangent to the brain surface. The angle of tilt was recorded using a digital protractor by measuring the tilt of the stereotaxic frame (Narishige) used to parallelize the frame relative to the table. The skull overlying visual cortex was carefully thinned with a dental drill, stopping often and rinsing with chilled artificial cerebral spinal fluid (ACSF, in mM: 125 NaCl, 10 d-glucose, 10 HEPES, 3.1 $CaCl_2$, 1.3 $MgCl_2$; or 150 NaCl, 2.5 KCl, 10 HEPES, 2 $CaCl_2$, 1 $MgCl_2$). Great care was taken to prevent overheating of the brain or subdural bleeding. The bone was thinned just past the spongy middle layer which often contained blood vessels. The resultant preparation was a thin layer of semi-flexible bone that was sufficiently transparent to reveal the brain's surface vasculature. This was especially relevant for alignment of cortical blood vessel landmarks with functional retinotopic maps. For calcium imaging experiments, a craniotomy was made to reveal the cortex for calcium indicator dye loading and subsequent two-photon imaging. After the surgery, chlorprothixene (2.5 mg/kg) was administered intramuscularly to the quadriceps and isoflurane was reduced to 0.25-0.8%, for visual stimulation and recording experiments. The

most robust visual responses coincided with higher respiration rates when the animal appeared to be lightly anesthetized.

Intrinsic Signal Optical Imaging

The intrinsic signal imaging protocol was adapted from previous studies (Kalatsky and Stryker, 2003; Nauhaus and Ringach, 2007). Imaging setup is as described in Nauhaus and Ringach, 2007. All other relevant modifications are described elsewhere in the text.

Dye Loading and Two-Photon Imaging

The retinotopic map from the intrinsic signal imaging experiment aligned and overlayed with the image of the cortical blood vessels from the same animal was used as a reference for targeting the locations of calcium-sensitive dye loading. The dye solution contained 1mM Oregon Green Bapta-1 AM (OGB, Invitrogen) with 10% DMSO and Pluronic F-127 in ACSF (Stosiek et al., 2003; Ohki et al., 2005). The solution also included 50 µM sulforhodamine-101 to selectively label astrocytes (Nimmerjahn et al., 2004). The pipette (3-5 µm outer diameter tip) was lowered diagonally (30° from horizontal) to 225 µm below the dura surface (layer 2/3) while short pulses of pressure were applied to the back of the pipette to keep the tip clear of debris. Then, a single pulse of 1 min duration and 10 PSI was applied for the loading protocol. This typically resulted in approximately 0.5-1 mm^2 of OGB loading. The loading was observed under epifluorescence to confirm sufficient dye injection. In most cases, several locations were injected in the same animal often using the same pipette multiple times, resulting in an area of OGB loading spanning up to several millimeters. Each loading site was separated by approximately 0.5-1mm. At least one hour after the last loading the two-photon imaging began.

A custom-built Movable Objective Microscope (Sutter) coupled to a Chameleon Ultra II mode-locked Ti:Sapphire laser (Coherent) was used for two-photon imaging. Standard wavelength for two-photon microscopy was 920-950 nm. A waveplate (Newport) was used in conjunction with a beamsplitter cube (Newport) to modulate the power of the excitation laser light. A 16X water-immersion objective (Nikon) was used for low magnification retinotopy experiments, and a 40X water-immersion objective (Olympus) was used to measure cellular responses. Fluorescent light was detected by photomultiplier tubes (Hamamatsu), after being filtered by one of two emission filter sets: HQ535/50, and HQ610/75 (Chroma). A third

acquisition channel was used to record the output of a photodiode to detect a brief pulse of light at the corner of the screen, which precisely indicated the phase of the periodic visual stimulus (e.g., drifting bar retinotopy stimulus), in addition to the stimulus beginning and end. ScanImage software (Pologruto et al., 2003) was used for image acquisition. Images and time lapse videos were processed offline in Matlab (MathWorks) and ImageJ (http://rsbweb.nih.gov/ij/). Imaging experiments were performed at ~130-180 µm below the dura surface (layer 2/3). For retinotopy experiments, images were typically acquired at approximately 2 Hz (256 x 256 pixel frames, unidirectional scanning, ~800 x 800 µm field of view for low magnification imaging with the 16X objective). For recording cellular responses, images were typically acquired at approximately 8 Hz (256 x 256 pixel frames, bidirectional scanning, either ~150 x 150 µm or ~300 x 300 µm field of view with the 40X objective). The 40X objective provided theoretically higher resolution than the 16X objective despite having identical numerical aperture (0.8 N.A.). This was because the 16X back aperture was under filled by the beam size possible on the microscope, reducing the effective N.A., whereas the 40X back aperture was over filled. For this reason, we used the 40X for cellular imaging experiments to obtain higher resolution. It should be noted that cellular responses were detected in our setup with the 16X objective, albeit with theoretically somewhat lower resolution. Different optics may make it possible to use the 16X alone for experiments of this nature. After each experiment in a given location, a stack of images (5 µm z step) was taken starting at the experiment image plane and ending above the dura in order to determine the precise depth of the experiment offline. Images were taken of the overlying surface blood vessel pattern in order to register images taken during experiments with the 40X objective with those with the 16X objective, and with the intrinsic imaging experiments. High-resolution images (1024 x 1024 pixel frames) were often taken of the experiment imaging plane as an anatomical reference of the cells recorded.

Visual Stimulation

Drifting bar and drifting grating stimuli were displayed on a gamma-corrected, large LCD display (68 x 121 cm, 120 Hz monitor, stimulus presented at 60Hz), rotated in ‘portrait’ mode such that the monitor was taller than it was wide, with the stimulus subtending 153 degrees of visual space along the vertical axis and 147 degrees along the horizontal axis. This results in a stimulus that is larger than the extent of the entire known visual hemifield of the mouse, which is

estimated to be at most 110 degrees vertical, 140 degrees horizontal (Wagor et al., 1980). The perpendicular bisector of the eye was defined as the origin of the line perpendicular to the screen that intersected with the center of the mouse's eye. This point defined 0° altitude and 0° azimuth of the stimulus.

The screen was placed at an angle of 20° relative to the animal around its dorsoventral axis such that the screen was pointed slightly inward toward the animal's nose. Since the eyes of the mouse point slightly inward towards the nose, this positioning ensures that the stimulus is approximately parallel to the retina, and properly stimulates the vertical meridian. The screen was also tilted to match the tilt of the animal relative to its normal position around its anteroposterior axis resulting from the angled placement of the recording chamber. For example, if the recording chamber was angled 20° from the normal horizontal plane of the mouse (as was necessary to access far lateral extrastriate areas), resulting in a corresponding tilt of the head when the chamber was held horizontal in the frame, the screen was also tilted 20° to ensure that the stimulus was parallel to the retina. Thus, in this configuration 0° altitude is defined as the plane passing through the center of the eyes parallel to the ground, even after the rotation is applied to the animal's head and the screen. It is important to note that the mouse's eyes are rotated slightly in the skull, so this definition of 0° altitude is not the center of the retina. Instead, we approximated the horizontal meridian to be approximately 20° altitude in this configuration. Thus 20° vertical (altitude) eccentricity should be considered the horizontal meridian in the retinotopic maps presented in this study (Figure 1, 2 and S2).

The screen was positioned so that the perpendicular bisector was 28 centimeters from the bottom of the screen, centered on the screen left to right (34 centimeters on each side), and 10 cm from the eye. This positioning of the monitor, in conjunction with the spherical stimulus correction described below, accurately simulated a hemispherical display around the mouse. This results in a stimulus that maintains constant spatial frequency at all locations. Furthermore, a distance of 10 cm between the eye and the stimulus is beyond the theoretical point of 'infinite focus' of the mouse eye (Remtulla and Hallett, 1985; Green et al., 1980; de la Cera et al., 2006), leading to similar focus at all points on the screen.

For both intrinsic imaging and low magnification calcium imaging retinotopy experiments, a periodic drifting bar stimulus was used (Kalatsky and Stryker, 2003). The bar was 20° wide and subtended the whole visual hemifield along the vertical and horizontal axes

(153° or 147° respectively). The bar was drifted 10 times in each of the four cardinal directions. A counter-phase checkerboard pattern was flashed on the bar, alternating between black and white (25° squares with 166 ms period) to strongly drive neural activity (Movie S1 and S2). Azimuth correction was used for the bar drifting along the horizontal axis and altitude correction was used for the bar drifting along the vertical axis (see below), in order to define eccentricity using standard spherical coordinates. By drifting the bar in both directions along a given axis it was possible to subtract the delay in the intrinsic signal relative to neural activity (Kalatsky and Stryker, 2003; see Data Analysis). The bar drifted at 8.5-9.5°/s for intrinsic imaging experiments and at 12-14°/s for two-photon imaging experiments.

For cellular resolution calcium imaging experiments, sinusoidal drifting gratings were used. For each population of neurons imaged (a single 40X imaging plane), we presented (with rare exceptions) four sets of stimuli: a temporal frequency varying experiment (0.5, 1, 2, 4 and 8 Hz, 8 directions plus blank, ~0.04 cpd, 5 repeats pseudorandomized for each parameter combination), a spatial frequency varying experiment (0.01, 0.02, 0.04, .08 and 0.16 cpd, 8 directions plus blank, ~1 Hz, 5 repeats pseudorandomized for each parameter combination), a 12 direction orientation tuning experiment (~1 Hz, ~0.04 cpd, 5 repeats pseudorandomized for each parameter combination and a blank condition), and a drifting bar retinotopy experiment (same stimulus as for the low magnification 16X retinotopy experiments). The retinotopic mapping experiment was performed with the 40x objective at cellular resolution to obtain a precise eccentricity value for each neuron in the field of view. This eccentricity value was used to restrict analysis to neurons with receptive fields within 50 degrees of the center of space, and ensure that the populations from each visual area represented similar regions of space (see Data Analysis section). A gray screen (mean luminance of grating stimuli) was shown between trials and during the prestimulus baseline period. Stimulus durations were 4 sec for the temporal frequency experiment and 2 sec for the spatial frequency and 12 direction experiments (Note: data are not presented for the 12 direction experiments). Population data from previous experiments in each area and from published data from V1 (e.g., Niell and Stryker, 2008) were used to determine the value for the parameters held constant in each experiment in an effort to strongly stimulate as large a population as possible, and keep parameters consistent across visual areas. An altitude correction was used to account for the spherical distortion of the flat monitor for spatial frequency, temporal frequency and orientation experiments. The isoluminance lines

of this stimulus are analogous to the altitude lines of a globe. That is, they form parallel rings that are evenly spaced in eccentricity. This correction held the spatial frequency and temporal frequency constant throughout the wide visual field.

Spherical corrections were applied to all stimuli in order to account for the distortions created by displaying stimuli to the animal on a flat monitor (Figure S1, Movie S1 and S2). Without correction, the spatial frequency and temporal frequency of a drifting grating shrink rapidly with eccentricity—a problem present in any study using a flat screen, but especially pronounced without appropriate correction in our study, which used a very large screen. Drifting bar and grating stimuli were generated through custom routines in Psychtoolbox and Matlab and then transformed with spherical projection, as described below.

Spherical Stimulus Correction

Retinotopic coordinates are often defined in units of degrees of visual field, a spherical parameter. However, monitors are flat, which means that spatial frequency (cyc/deg) and speed (cyc/sec) become gradually reduced for larger eccentricities when they are kept constant in cycles/centimeter. When the eccentricities are kept to reasonably low values (e.g. $<30^o$), this distortion is small. However, our experiments call for stimulation over a large enough region of visual space that this distortion becomes quite substantial. For example, a drifting bar that is kept constant in its width (cm) and speed (cm/sec) will become dramatically smaller (degrees) and slower (deg/sec) at the largest eccentricities of our stimulus. We thus defined our stimuli such that the angular variables in spherical coordinates (altitude or azimuth) are the independent variables. For example, our sine wave gratings were defined as a function of spherical variables, and these values were then projected onto a flat surface.

In our 3-dimensional coordinate system, we defined the eye as the origin. For the reasons described above, our desired visual stimuli are initially described as a function of altitude, θ, and azimuth, ϕ: $S(\theta,\phi)$. The spherical coordinate space is oriented such that the perpendicular bisector from the eye to the monitor is the $(0^o,0^o)$ axis of the altitude/azimuth coordinates, altitude increases above the mouse, and azimuth increases anterior to the mouse. Next, we convert these spherical coordinates to Cartesian coordinates so that they can be drawn on the monitor. To do so, we orient the Cartesian space so that the perpendicular bisector between the

eye and the monitor is the x-axis. The y and z axes are defined as the horizontal and vertical dimensions on the monitor, with the x-dimension a constant on the monitor surface (x_o). We can now define the stimulus as a function of the horizontal (y) and vertical (z) pixel locations:

$$S(\theta(x_o,y,z),\phi(x_o,y,z)) = S(\frac{\pi}{2} - \cos^{-1}(z/\sqrt{x_o^2+y^2+z^2}) \ ,\tan^{-1}\left(\frac{-y}{x_o}\right))$$

Next, we define a drifting grating that is a function of altitude, θ , and constant in ϕ. We start with $S = \cos(2\pi f_s\theta - tf_t)$, where '$f_s$' is the spatial frequency (cycles/radian), 'f_t' is the temporal frequency (radians/second), and 't' is time. We then apply the polar-to-Cartesian transformation, which gives us

$$\cos(2\pi f_s(\frac{\pi}{2} - \cos^{-1}(z/\sqrt{x_o^2+y^2+z^2})) - tf_t)$$

To change the 'orientation' of the drifting grating, we rotate it counterclockwise around the x-axis. This is done by applying a rotation of the y/z plane, which can be obtained by redefining y in the above equation as

$$z*\sin(-\varphi) + y*\cos(-\varphi), \text{ and z as } z*\cos(-\varphi) - y*\sin(-\varphi).$$

We have thus defined a drifting grating with contours along altitude lines that have been oriented by 'φ'. The stimulus is drawn on the monitor using the y and z domains.

Data Analysis

Intrinsic optical imaging retinotopy data were analyzed as previously described (Kalatsky and Stryker, 2003). Briefly, data were acquired in a continuous block during stimulus presentation of a bar drifting in one direction periodically. The phase of response relative to the stimulus was computed for each pixel by computing the phase of the Fourier component at the same frequency as the stimulus. Contrasting this phase difference with the data from the bar drifting in the opposite direction along the same axis made it possible to estimate the center point between them, accounting for the hemodynamic delay, and thus determining the best estimate of the position in space that the cortical location responded to. A comparable approach was used to analyze Ca^{2+} imaging retinotopy experiments.

For population analyses of cellular responses to drifting gratings, data were preprocessed in the following ways. Each experiment (e.g., temporal frequency varying experiment) typically lasted approximately 30-45 minutes. To account for drifts in the image over time, we applied a movement correction algorithm that aligned each trial of the experiment to the average image of the first trial by determining the highest cross-correlation between the images. Then regions of interest (ROIs) around each cell in the image were created using a semi-automated procedure, separately for the OGB channel (neurons and glia) and the sulfarhodamine-101 channel (glia). Candidate ROIs were determined by thresholding an image of the field of view that had first been processed with a local Z-score to normalize the local statistics. Then, ROIs were carefully edited manually for both channels. Glia cells were removed from the analysis of the OGB channel by removing any ROIs in the OGB channel that overlapped with ROIs marked in the glia channel. The remaining ROIs in the OGB channel were neurons. The pixels were averaged within each of these ROIs for each time point (each single image) to reflect the raw time course of a given neuron.

In order to link neuron identities across experiments (e.g., to perform spatial and temporal frequency cell-by-cell correlations), we found the relative position between the ROI maps for each experiment that maximized the cross-correlation. Then we determined the cell ROIs which overlapped across the ROI maps for each experiment by at least 3 pixels (the great majority of neurons were overlapping) and created a new ROI map with unique identifiers of each common neuron. Inverse transformations were applied to each ROI map so that each map realigned with each original experiment. The end result was a common ROI map that identified neurons across multiple experiments within the same field of view that accounted for any drifts in the imaging field of view over the course of the imaging session.

The baseline calcium fluorescence signal was averaged within each cell ROI for each trial during a prestimulus period during which a gray screen was shown (1 sec). Then, the entire time course was converted from absolute fluorescence values to the percent change relative to baseline by computing the following: $\mathbf{\Delta F/F = (F_I\text{-}F)/F}$, where F_I is the instantaneous fluorescence signal and F is the baseline fluorescence. The $\Delta F/F$ response for each cell was averaged during a two-second window following stimulus onset for each trial, and the mean and standard deviation across trials for each stimulus and blank condition were computed for each neuron. We applied several criteria to include neurons in further population analyses. Neurons

were deemed visually responsive if they gave a mean response above 6% ΔF/F to any of the stimuli. A response reliability metric ($\boldsymbol{\delta}$) was computed for each neuron as follows:

$$\delta = \frac{\mu_{max} - \mu_{blank}}{\sigma_{max} + \sigma_{blank}}$$

where $\boldsymbol{\mu_{max}}$ and $\boldsymbol{\sigma_{max}}$ are the mean and standard deviations of the response to the preferred stimulus respectively, and $\boldsymbol{\mu_{blank}}$ and $\boldsymbol{\sigma_{blank}}$ are the mean and standard deviations of the response to the blank stimulus respectively. Neurons were deemed reliable for $\boldsymbol{\delta} > 1$. Finally, neuron eccentricity mapped with the retinotopy stimulus was used to restrict our population analyses to eccentricity-matched neurons within 50° of the center of space (see Table S1). The numbers of neurons which met all of these criteria were used as the denominator in all subsequent analyses of fraction of neurons exhibiting a particular score on a given parameter.

Tuning Metrics

Temporal and spatial frequency tuning curves were taken at the optimal orientation and direction for each neuron, using the average ΔF/F response for each condition across trials. These tuning curves were fit with a Difference of Gaussians function (Sceniak et al., 2002). A $\log_2$ transform was performed on the x-axis of the curves, converting it to octaves. The preferred frequency was taken at the peak (maximum) location of this curve. For bandwidth and low and high cutoff measurements, each cell was characterized as either bandpass, highpass or lowpass for temporal and spatial frequency based on whether its minimum and/or maximum frequency response passed below the half max for the tuning curve. The high cutoff was computed for bandpass and lowpass cells as the highest frequency which drove a half-max response. Low cutoff was computed for bandpass and highpass cells as the lowest frequency which drove a half-max response. Bandwidth was measured for bandpass cells as the difference between high cutoff and low cutoff.

The orientation and direction tuning curves were taken at the optimal spatial frequency for each neuron, using the average ΔF/F response for each condition across trials. The orientation selectivity index (OSI) was computed as follows:

$$OSI = \frac{\mu_{max} - \mu_{orth}}{\mu_{max} + \mu_{orth}}$$

where $\boldsymbol{\mu_{max}}$ is the mean response to the preferred orientation and $\boldsymbol{\mu_{orth}}$ is the mean response to the orthogonal orientation (average of both directions). The direction selectivity index was computed as follows:

$$DSI = \frac{\mu_{max} - \mu_{opp}}{\mu_{max} + \mu_{opp}}$$

where $\boldsymbol{\mu_{max}}$ is the mean response to the preferred direction and $\boldsymbol{\mu_{opp}}$ is the mean response to the opposite direction. The half-width at half-maximum (HWHM) was computed for each neuron's orientation and direction tuning curves but our results suggested that we did not adequately sample the direction domain to make comparisons based on these measurements (i.e., neurons may have had sharper tuning widths than our sampling of the direction domain could detect).

Statistics

We started with the most basic question: are mouse cortical visual areas distinguishable based on population tuning metrics? We asked this question statistically using a multivariate analysis of variance (MANOVA) on the four values we computed for every neuron in our sample from each area: preferred temporal frequency, preferred spatial frequency, orientation selectivity index and direction selectivity index. We also computed bandwidth and high and low cutoff metrics for each population, however not every neuron received a value for all of these metrics and thus we excluded these metrics from the multivariate analysis. We followed up this analysis with individual univariate analyses to confirm whether there was a main effect of area on each of our dependent variables (both one-way ANOVA and one-way Kruskal-Wallis tests). Finally, for each significant one-way test, we performed post-hoc pairwise comparisons to determine which areas were different from each other in terms of each metric, correcting the p value for multiple comparisons using the Tukey-Kramer Honestly Significant Difference (HSD). Pearson correlation coefficients and statistical significance compared against no correlation were computed using Matlab routines, and the p value was corrected for multiple comparisons using the Bonferroni method (Figure S6).

III. Supplemental References

Pologruto, T.A., Sabatini, B.L., and Svoboda, K. (2003). ScanImage: flexible software for operating laser scanning microscopes. Biomedical engineering online *2*, 13.

Remtulla, S., and Hallett, P.E. (1985). A schematic eye for the mouse, and comparisons with the rat. Vision Res *25*, 21-31.

Green, D.G., Powers, M.K., and Banks, M.S. (1980). Depth of focus, eye size and visual acuity. Vision Res *20*, 827-835.

de la Cera, E.G., Rodriguez, G., Llorente, L., Schaeffel, F., and Marcos, S. (2006). Optical aberrations in the mouse eye. Vision Res *46*, 2546-2553.